



Scalable Electrospinning Methods to Produce High Basis Weight and Uniform Drug Eluting Fibrous Biomaterials

Jamie L. Hernandez, My-Anh Doan, Ryan Stoddard, Hannah M. VanBenschoten, Shin-Tian Chien, Ian T. Suydam and Kim A. Woodrow*

Department of Bioengineering, University of Washington, Seattle, WA, United States

Electrospinning is a process for fabricating nonwoven fibrous materials of versatile composition and form that has shown enormous promise as medical wound dressings, tissue engineered scaffolds, and for pharmaceutical delivery. However, pharmaceutical application and clinical translation of electrospun fibers requires a scalable process to control mass deposition and uniformity in the finished materials. Here, we show that free-surface electrospinning using a stationary wire electrode can generate fiber materials with high productivity and controllable deposition to achieve uniform area density (basis weight) that is relevant for scalable pharmaceutical dosage form production. Using a production-scale instrument, we performed statistically designed optimization experiments to identify a combination of parameters that improved productivity up to 13 g/h. By combining this optimization with process controls for dynamic movement of the electrospinning substrate, we also demonstrate the production of uniform and high area density materials of 50–120 G per square meter. We verified our process by fabricating a triple drug solid dosage form at a high area target density (100 g/m²) that largely showed less than a 10% coefficient of variation in mass or drug content. The process developed here provides a general approach for optimizing different material compositions for high productivity and uniformity, and advances the use of free-surface electrospinning for manufacturing fiber-based biomedical materials.

Keywords: electrospinning, basis weight, Design of Experiments (DoE), solid dosage form, scale-up, drug delivery

OPEN ACCESS

Edited by:

Silviya Petrova Zustiak,
Saint Louis University, United States

Reviewed by:

Giuseppe Tronci,
University of Leeds, United Kingdom
Paola Ginestra,
University of Brescia, Italy

*Correspondence:

Kim A. Woodrow
woodrow@uw.edu

Specialty section:

This article was submitted to
Delivery Systems and Controlled
Release,
a section of the journal
Frontiers in Biomaterials Science

Received: 25 April 2022

Accepted: 10 June 2022

Published: 11 July 2022

Citation:

Hernandez JL, Doan M-A, Stoddard R,
VanBenschoten HM, Chien S-T,
Suydam IT and Woodrow KA (2022)
Scalable Electrospinning Methods to
Produce High Basis Weight and
Uniform Drug Eluting
Fibrous Biomaterials.
Front. Front. Biomater. Sci. 1:928537.
doi: 10.3389/fbiom.2022.928537

INTRODUCTION

Nonwoven textiles have shown broad applicability for biomedical research. Electrospinning is one notable nonwoven fabrication method that is especially promising due to the versatility of composition and form of the finished materials. Physiochemically diverse pharmaceutical actives and excipients can be formulated into a wide-range of polymer materials (Blakney et al., 2013; Chou et al., 2015; Blakney et al., 2016; Carson et al., 2016; Stoddard et al., 2016; Blakney et al., 2017). In addition, the electrospinning process allows for tuning of fiber size and alignment as well as bulk material properties such as microstructure, topography, and mechanics (Deitzel et al., 2001; Sill and von Recum, 2008; Chou et al., 2015; Wang et al., 2016; Chen et al., 2018; Feng et al., 2019; Xue et al., 2019). The ability to control the composition and form of electrospun materials is advantageous as these properties can significantly affect their performance, which has attracted their use in a variety of

pharmaceutical and clinical applications (Sill and von Recum, 2008; Persano et al., 2013; Stoddard et al., 2016; Feng et al., 2019; Xue et al., 2019).

Despite the adaptability of electrospinning, a scalable process that is sufficiently productive and produces uniform materials at controllable densities is needed for clinical translation (Stoddard et al., 2016; Tuin et al., 2016; LeCorre-Bordes et al., 2017). Laboratory-scale electrospinning is commonly performed using a single charged needle with low-throughput of 1–100 mg/h and yields a relatively small area of low-density uniform material (Huang et al., 2019). Several innovations in fabricating polymer fibers by electrospinning have emerged over the decades, but scalable production has been limited to only a few processes with commercial instruments (dos Santos et al., 2020). Multi-needle and needleless electrospinning lead the field in production- and industrial-scale instruments. Free-surface electrospinning has several advantages over multi-needle modalities and improves material throughput by promoting formation of numerous polymer jets from a charged surface like a wire or cylinder (Krogstad and Woodrow, 2014). Industrial free-surface electrospinning instruments are capable of productivity rates up to 300 g/h (Huang et al., 2019). Free-surface electrospinning has also shown the capacity to produce materials composed of protein solutions relevant to food packaging and healthcare applications (Basel Bazbouz et al., 2018; Botelho Moreira et al., 2019). However, all scalable electrospinning processes to date yield materials with low area density or basis weight in the range of 0.02–10 g/m² (gsm) (Stoddard et al., 2016; Tuin et al., 2016; Huang et al., 2019). For clinical applications, low density electrospun materials may increase the required dose and affect performance of the finished product. As such, a singular scalable process that is productive and allows for precise control of area density and uniformity is highly desirable for clinical translation of electrospun materials.

Here, we establish a process for fabricating uniform and high area density electrospun fiber materials by free-surface electrospinning using an oscillating carriage for solution entrainment onto a stationary wire electrode. Using this free-surface electrospinning modality, we performed statistically designed screening experiments that identified individual and combined factors that contribute to fiber throughput and deposition. We also implemented a process for dynamic movement of the collection substrate to control material density and uniformity. Finally, we verified our process and control optimizations by fabricating a triple drug solid dosage form at a high area target density that we assessed for throughput and dose uniformity. By combining our optimization with process controls, we show the ability to produce high area density materials of 50–120 G per square meter and obtain productivity of up to 13 g/h on a production-scale instrument. We also successfully demonstrate co-formulation of physicochemically diverse drugs into a single fiber-dosage at a target 100 g/m² with low coefficient of variation in mass or drug content. The process developed here yields the highest basis weight electrospun fibers for drug delivery to our best knowledge (Stoddard and Chen, 2016; Tuin et al., 2016; Zhang et al., 2017; Huang et al., 2019) and provides a general approach

for optimization of any material composition for high productivity and uniformity.

MATERIALS AND METHODS

Materials

Polymers polyvinyl alcohol (PVA, 87%–90% hydrolyzed, Mw = 30,000–70,000, Sigma Aldrich), polyethylene oxide (PEO, Mw = 400,000, Scientific Polymer Products, Inc.), polylactic-co-glycolic acid (PLGA, 50:50 L:G, carboxylate terminated, inherent viscosity = 0.55–0.75 dl/g, Lactel Absorbable Polymers), and poly-L-lactic acid (PLLA, ester terminated, inherent viscosity = 0.90–1.20 fl/g, Lactel Absorbable Polymers) were electrospun with either deionized water, hexafluoroisopropanol (HFIP), or a mixture of chloroform and 2,2,2-trifluoroethanol (2,2,2-TFE)/HFIP (Oakwood Chemical) and collected onto industrial brown waxed paper (24" × 1,500', 30 lb) as the electrospinning substrate. Antiretroviral (ARV) agents were purified as described in Jiang, et al. from tablets of Selzentry[®] (300 mg, ViiV Healthcare), Insentress[®] (400 mg, Merck), and Intelence[®] (200 mg, Janssen) for maraviroc (MVC), raltegravir (RAL), and etravirine (ETR), respectively (Jiang et al., 2015). Sieved Tenofovir (TFV, Particle Sciences, gift from CONRAD) was used as obtained. Dimethyl sulfoxide (DMSO, BDH/VWR Analytical), acetonitrile (HPLC grade, Sigma-Aldrich), and potassium monophosphate (Fisher Chemical) were used for quantification.

Polymer Formulation and Characterization

Unless otherwise specified, PVA/PEO was formulated at 84:14 (w/w) PVA and PEO and 17.4% (w/v) in deionized water. Polymers were mixed using a stand mixer (Eurostar 20 digital, IKA) at 1,000 RPM for 10 min, then 100 RPM overnight. PLGA fibers were electrospun from a 15% (w/v) PLGA solution in HFIP and mixed with a stir bar overnight. For drug loaded formulations, each agent was homogenized (T25 digital Ultra-Turrax, IKA) into the solvent prior to addition of polymer, at the specified loading percentage.

Free-Surface Electrospinning

All electrospinning was conducted using a Elmarco Nanospider (Liberec, Czech Republic) with an oscillating carriage electrospinning electrode. In this method, fibrous materials are generated from a polymer solution that is coated onto a wire electrode by an oscillating carriage. The carriage holds a reservoir filled with the polymer solution and coats the wire through an interchangeable orifice in which the wire passes through. Solid fibers are formed from this solution by an applied voltage gradient across the wire electrode and collection electrode. The collection electrode is covered by the collection substrate to allow for simple collection of the material. This substrate can undergo dynamic movement during the electrospinning process.

Unless specified, solutions were coated onto the wire electrode through a 0.7 mm orifice at a rate of 350 mm/s. Additionally, the collection electrode was maintained at a distance of 200 cm, and electrospun across a 100 kV voltage difference. Chamber humidity was controlled at approximately 10% using

compressed air. Waxed paper was used as the collection substrate. Under static electrospinning conditions, the collection substrate remained stationary. Under dynamic electrospinning conditions, the collection substrate was translated at a rate of 155 mm/min. This movement oscillates over a defined distance, labeled to start (marker 1) and end (marker 2) directly above the wire electrospinning electrode, and continuously pass over this defined distance. A single pass is defined when the first marker labeled on the collection substrate and aligned directly above the wire electrode (Material direction (MD) axis = 0), is translated until the second marker, at specified dynamic path length (DPL) away from the first marker, is aligned with MD = 0. The next pass is performed with the reversed movement of the collection substrate until the first marker has returned to the starting position. Electrospinning was conducted until the center fiber mass reached a target basis weight of 100 gsm. This target was determined through periodic sampling of the center-most 4 × 4 cm fiber section, which was removed, weighed, and replaced for further electrospinning. Additional electrospinning time or pass number was then determined by linear interpolation.

Throughput, Mass Distribution Analysis, and Simulations

Throughput was measured by the mass of the fibers collected on the pre-weighed substrate divided over time. Samples of the fiber mats were collected with a 1 cm arch punch tool ($7.85 \times 10^{-5} \text{ m}^2$) at specified locations and weighed with a microbalance (Mettler Toledo). The value σ_s is determined from gaussian line fitting from $n = 5$ samples which were collected across the carriage direction (CD) averaged at both edges. To determine gaussian line fits across the material direction (MD) of the fiber mat, statically spun materials were sampled. Using these gaussian line fits, simulations were created to model dynamic electrospinning conditions, where the electrospinning substrate translates to increase the collected surface area of fibers. In addition to gaussian line fit equations, simulations also accounted for the electrospinning substrate winding rate and approximate fiber deposition per pass. Simulations of mass deposition and correlations to measured mass deposition were conducted using MATLAB (MathWorks Inc, Natick, MA, USA, version R2019b).

Quantification of Drug Content Using HPLC

Fiber samples were dissolved in DMSO at a concentration of 1 mg fiber/ml. Samples of the solutions were filtered with 0.22 μm syringe filters (Millex Durapore, Millipore) prior to quantification. High-performance liquid chromatography (HPLC, Shimadzu Prominence) was then used to measure the concentrations of the three drugs in tandem with a diode array detector (Shimadzu Prominence SPD-20A). Samples were analyzed at 35°C at a flow rate of 1 ml/min, and a gradient of 38%–73% acetonitrile (ACN) and 25 mM monopotassium phosphate in water (KH_2PO_4 buffer) was used as the mobile phase. Specifically, the mobile phases begin at a ratio of 62:38 KH_2PO_4 buffer/ACN, then ACN increases to 73% of the mobile phase over 8 min, and then is returned to 38% by the end of the

20 min sample run. A C18 column (5 μm , 100 Å, 250 × 4.6 mm, Phenomenex Kinetex) is used as the stationary phase. Detection wavelengths and approximate retention times were 193 nm and 4.3 min for MVC, 300 nm and 7.1 min for RAL, and 234 nm and 15.3 min for ETR.

Statistical Analysis

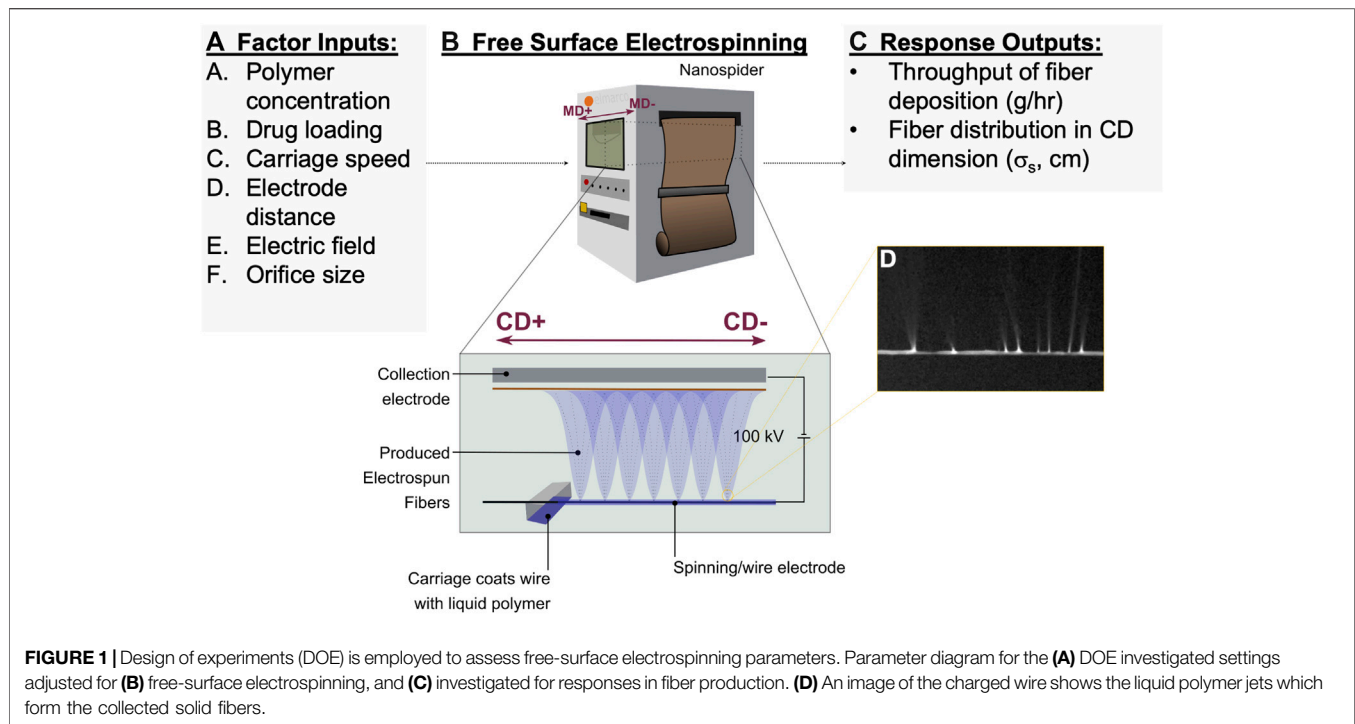
Planning and analysis for the statistically designed optimization experiments was conducted using StatEase Design-Expert (Minneapolis, MN, USA, version 9.0.4.1). Linear and gaussian line fits, as well as determinations of statistical significance were made using GraphPad Prism (San Diego, CA, USA, version 9). Significant differences were determined using repeated measured two-way ANOVA, or repeated measures one-way ANOVA for overall drug loading comparisons, with Geisser-Greenhouse correction and with Tukey's multiple comparisons test.

RESULTS

Assessment of Electrospinning Parameters on Fiber Throughput and Distribution

Free-surface electrospinning is amenable to scale-up, but the process has been used primarily in low-basis weight coatings for industrial filtration. Therefore, we first set out to optimize processing parameters for free-surface electrospinning that would achieve the high basis weight and uniformity required for pharmaceutical manufacturing of biomedical materials. Design of experiments (DOE) was used to efficiently identify process and solution parameters that would significantly affect fiber yield and distribution (**Figure 1A**). Factor inputs included polymer concentration (0.174–0.196 g/ml) and drug loading of a model agent tenofovir (0–28.57%, or 0–10 M). We also investigated the effect of four process variables: carriage speed coating the polymer solution onto the charged stationary wire (125–250 mm/s), distance between the charged electrospinning wire and oppositely charged electrospinning substrate (180–220 mm), applied electric field (0.35–0.45 kV/mm), and size of the orifice out of which the polymer solution flows onto the charged wire (0.6–0.8 mm). The specific polymer formulation used for parameter optimization was composed of PVA and PEO at a ratio of 84:14, which was determined independently via hill-climbing optimization (Skiena, 2008).

Electrospinning experiments with the specified factor input settings were performed on an Elmarco Nanospider (**Figure 1B**). The location of the collected material was defined with respect to the carriage direction (CD) and the material direction (MD) of the instrument. CD is defined as the axis parallel to the wire electrospinning electrode, where the carriage translates across to re-coat the wire with polymer electrospinning solutions (**Figure 1B**). MD is perpendicular to the CD-axis and defined as the direction in which the electrospinning substrate translates. We determined that a scalable method for producing medical materials will require dense and uniform accumulation of material within a reasonable time frame. As such, we focused



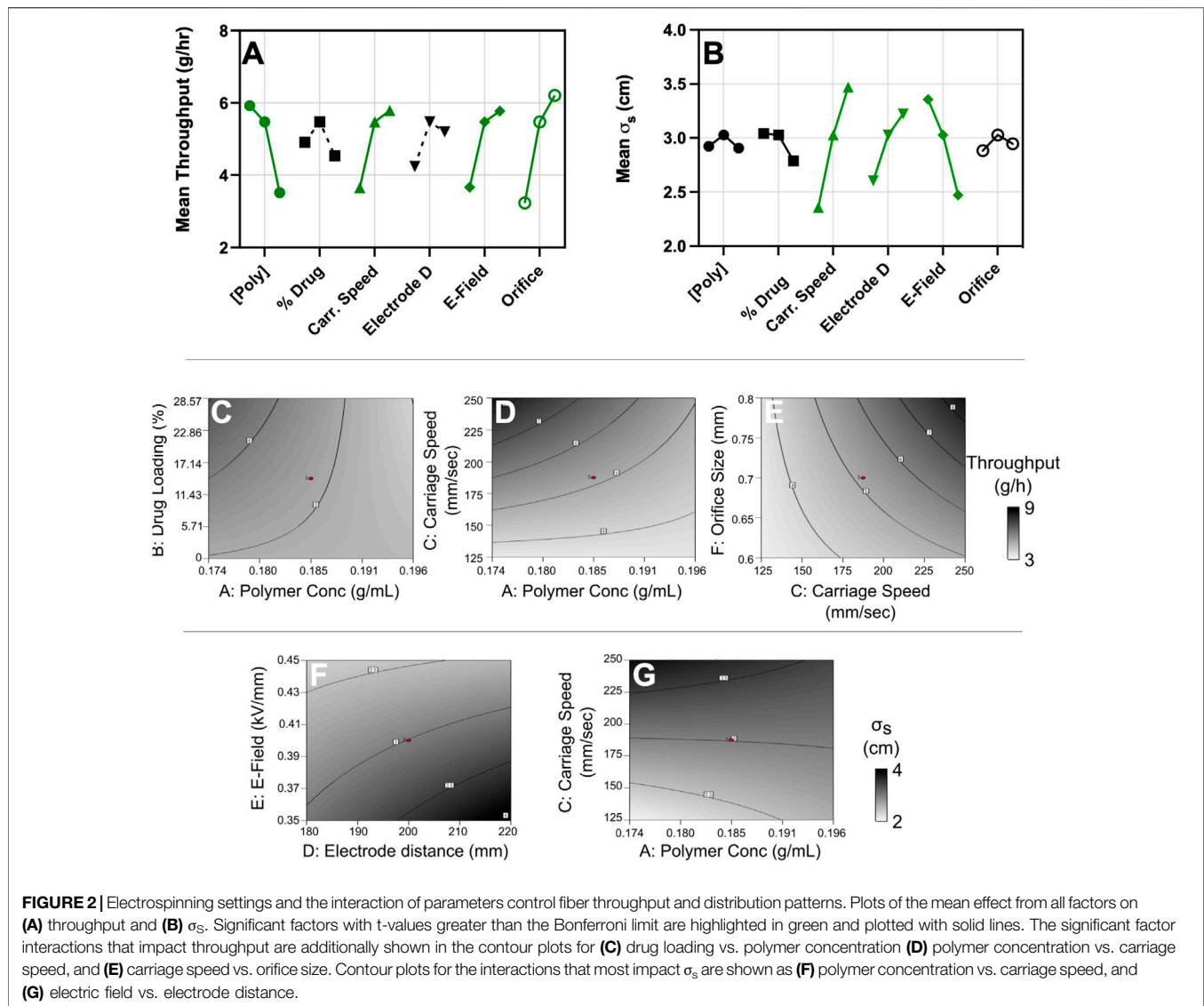
on fiber throughput (units of g/m^2 , or gsm) and fiber distribution measured along the CD-axis (σ_s , in cm) (Figures 1C,D).

Carriage speed, polymer concentration, orifice size, and electric field all significantly impact fiber throughput (Figure 2A; Supplementary Figure S1A). Indeed, low polymer concentration, high carriage speed, high orifice size and high electric field yielded the greatest throughput of 12.9 g/h. Fiber distribution was most significantly affected by carriage speed, electric field, and electrode distance (Figure 2B; Supplementary Figure S1B). With a high carriage speed, high electrode distance, and low electric field, the greatest σ_s value of 5.11 cm was achieved. Several two-factor interactions showed significant effects on the throughput and distribution response outputs (Supplementary Tables S1, S2). Throughput significantly increased with the interaction of increased drug loading and decreased polymer concentration (Figure 2C), decreased polymer concentration and a higher carriage speed (Figure 2D), as well as a higher carriage speed and larger orifice (Figure 2E). Several two-factor interactions were found to significantly effect σ_s (Supplementary Figure S1B; Supplementary Table S2). The σ_s value increased with interactions between low polymer concentration and high carriage speed (Figure 2F), as well as a decreased electric field and larger electrode distance (Figure 2G). We conclude that the optimal electrospinning parameters for our experiment would have a lower polymer concentration (0.174 g/ml), higher carriage speed (250 mm/s), an electrode distance of 200 mm, an applied 100 kV voltage difference, and an orifice size of 0.7 mm. Since the electric field had opposing impacts on throughput and distribution, we opted to use a

higher electric field to prioritize productivity, and compensate for deposition consistency by controlling substrate movement.

Dynamic Substrate Movement for Controlling Uniform Fiber Deposition

Free-surface electrospinning supports greater scalability of fiber production due to the higher density of fiber jets and adaptability for roll-to-roll processing. We took advantage of the ability to control the movement of the collection substrate along the MD axis to obtain high-basis weight and uniform materials. By controlling the residence time and substrate movement relative to the electrospinning wire, we could precisely tune fiber collection in specific areas. Figures 3A,B illustrate the difference in fiber deposition under electrospinning conditions with a static or dynamic collection substrate, respectively. We hypothesized that longer residence times achieved by repeated “passes” of the collection substrate across a specified dynamic path length (DPL) could increase the basis weight or accumulation of fibers across a larger area. Here, we define the DPL as the distance of the collection substrate that repeatedly and directly passes over the wire electrospinning electrode (Figure 3B). In addition to the polymer blend previously optimized for fiber throughput, we assessed a polymer solution composed of 15% (w/v) PLGA in HFIP. We selected this material for the differential use of an organic solvent, common use of HFIP with electrospinning, and the common use of PLGA in biomedical applications. We expect the use of these different polymer solutions illustrates the resulting differences in electrospinning, as well as the general application of these simulations as a tool to account for differences in fiber deposition.



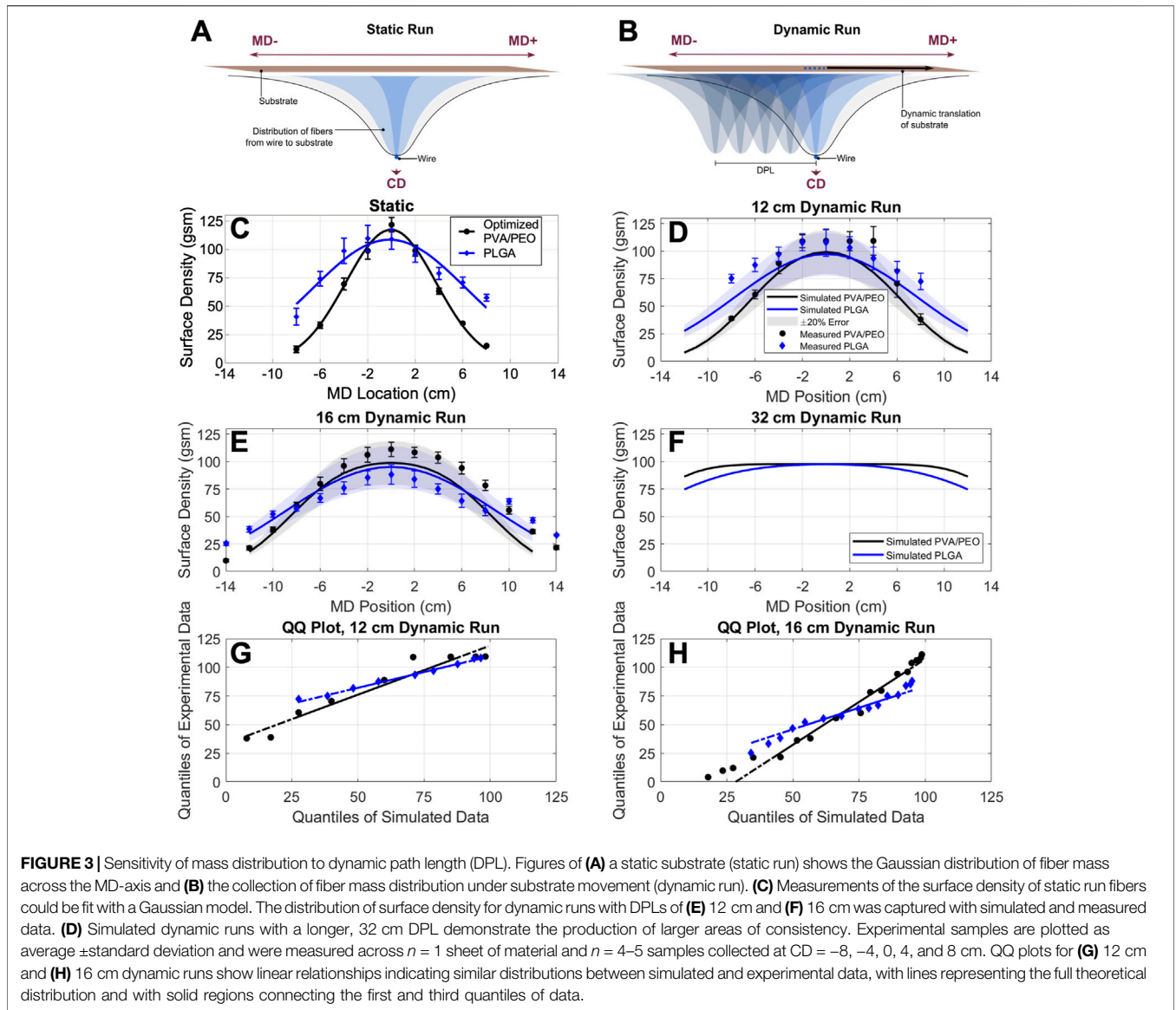
Electrospun fibers collect with variable deposition along the MD and away from the electrospinning electrode, as seen under static electrospinning conditions (**Figure 3A**). For a fixed position on the CD-axis, electrospun fibers were found to deposit with a Gaussian distribution across the MD-axis, centered at the wire electrospinning electrode ($MD = 0$ cm). Simulating material deposition can therefore inform necessary electrospinning parameters needed to achieve defined areas with uniform fiber basis weight. Therefore, the resulting fiber basis weight (A , in gsm) as a function of MD position (x_{MD} , in cm) under static conditions can be described by the following equation:

$$A(x_{MD}) = A_{Target} e^{-\frac{1}{2} \left(\frac{x_{MD} - \mu}{\sigma_{MD}} \right)^2}$$

The maxima of fiber deposition is equivalent to the target fiber basis weight (A_{target}), which we set to 100 gsm, and controlled for

during electrospinning by periodic sampling of the centermost 4×4 cm square of material. Due to this method for controlling material deposition, samples with coordinates at the edge of this testing region ($MD = \pm 2$ cm, $CD = \pm 2$ cm) could not be accurately collected. We additionally maintained center coordinates during dynamic electrospinning such that the MD position of the mean basis weight (μ) is equal to zero. Most interestingly, we found that the standard deviation of this Gaussian fiber-mass distribution (σ_{MD} , in cm) – or the spread of fiber deposition across the MD-axis – varies based on the polymer formulation. Under static electrospinning conditions, the observed spread of fiber deposition was found to be smaller, or narrower, for PVA/PEO ($\sigma_{MD} = 3.787$ cm) than PLGA ($\sigma_{MD} = 6.443$ cm) (**Figure 3C**; **Supplementary Table S3**).

It might be hypothesized that a formulation with a larger σ_{MD} value, and therefore wider fiber distribution, may yield fiber mats with a larger region of uniform fiber deposition at the target basis

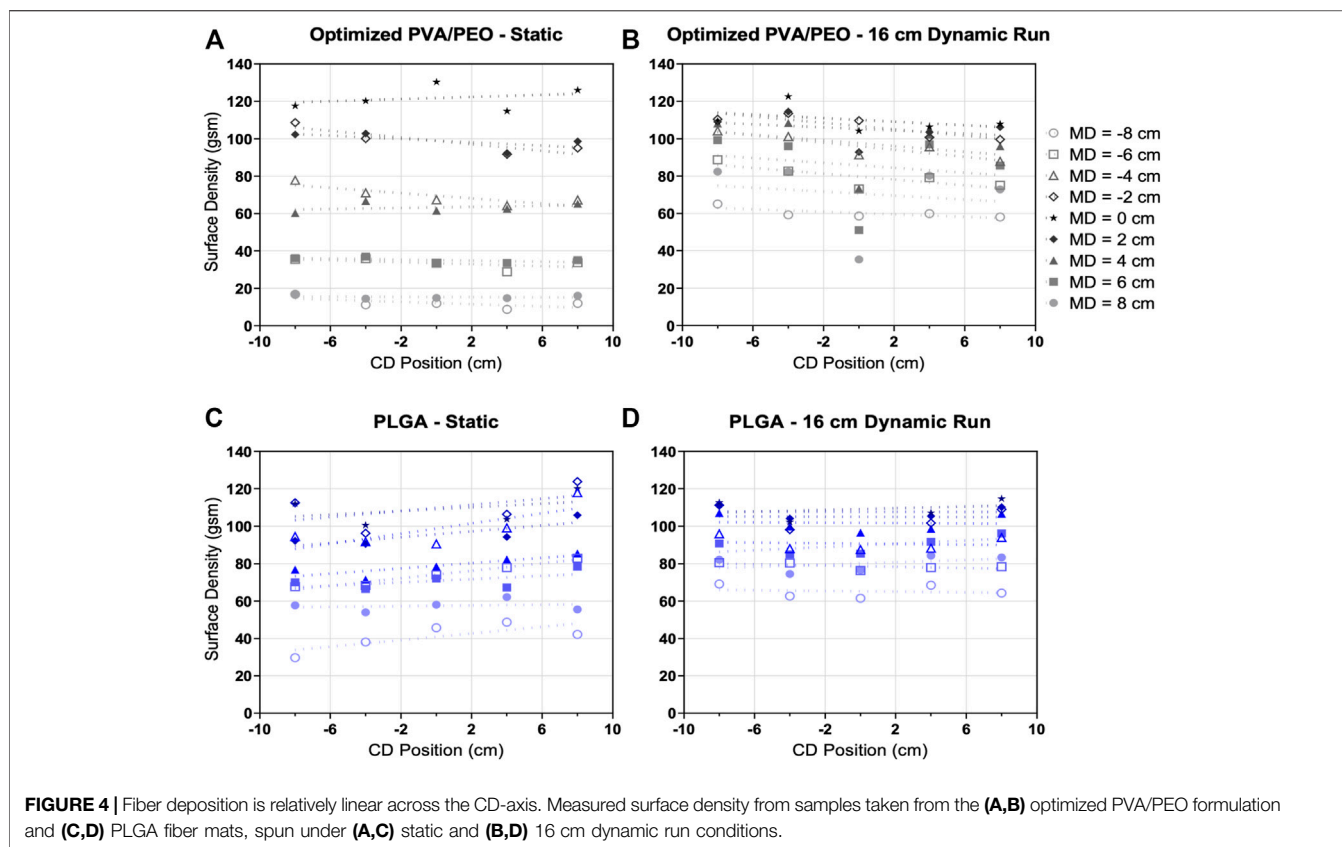


weight under dynamic electrospinning conditions. However, fiber deposition simulations do not reproduce this expectation. Simulated data was produced using the equation below, where p is the pass number of the substrate above the wire electrode, DPL is defined as the difference of the starting position ($l_{p, st}$) and the ending position ($l_{p, ed}$) centered at MD = 0, r_{sub} is the rate of substrate movement (155 mm/min), t_{stat} is the time to 100 gsm determined from the static run, and k is the step in MD position away from the center of the wire electrode. With a shorter DPL such as 12 cm, the PVA/PEO formulation with the lower σ_{MD} indeed yields a fiber sheet with a smaller uniform area than the PLGA formulation (Figure 3D). However, DPLs approximately 16 cm and larger can be seen to have a larger uniform area for formulations with a lower σ_{MD} compared to higher σ_{MD} values (Figures 3E,F). This is because the target 100 gsm basis weight is controlled for in all materials at the center of the mat. Therefore, as the path becomes increasingly large, formulations with larger

σ_{MD} values achieve the target basis weight at the center with fewer passes, and have a shorter electrospinning time for fibers to accumulate.

$$\max_{p=1} \left\{ p \times \sum_{k=l_{p, st}}^{l_{p, ed}} \left(\frac{1}{r_{sub} t_{stat}} \right) A_{Target} e^{-\frac{1}{2} \left(\frac{x_{MD}-k}{\sigma_{MD}} \right)^2} \right\} \leq 100 \text{ gsm}$$

Differences in fiber distribution were also observed between different polyester formulations. Using another polyester, poly L-lactic acid (PLLA), we electrospun solutions with different polymer concentrations and organic solvent properties. PLLA electrospun under 16 cm dynamic run conditions differs in its fiber distribution ($\sigma_{MD} = 8.813$ cm) compared to PLGA spun under similar conditions ($\sigma_{MD} = 9.277$ cm) (Supplementary Figures S2A, S2B). Though both are polyesters, PLLA has a slightly narrower distribution, confirming our findings that



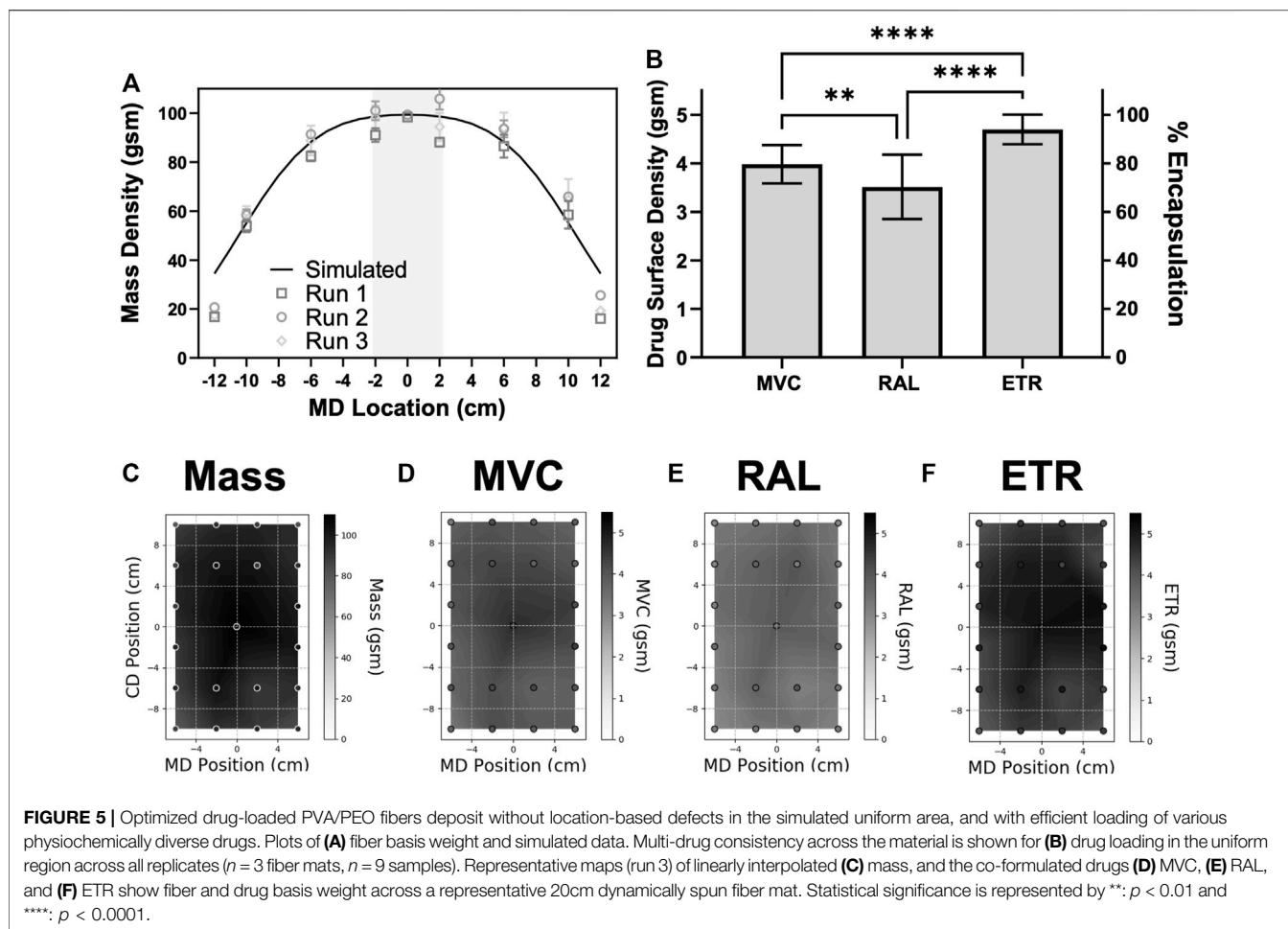
polymer type influences fiber uniformity. Moreover, in agreement with our DOE, PLLA fiber uniformity, albeit in the MD direction rather than CD direction, is significantly affected by the incorporation of TFE as a cosolvent compared to HFIP (Supplementary Figures S2B vs. S2C) and by lowering the polymer concentration in solution from 15% w/v to 10% w/v (Supplementary Figures S2B vs. S2D). This potentiates the results of our DOE to inform scale-up in dynamic run settings for a variety of polymer types and illustrates the importance of compatible solvent selection.

Simulations proved to be a useful tool for predicting fiber deposition patterns of different polymer formulas, and especially the region in which mass deposition plateaus. We found experimental data to be highly correlated to simulated dynamic run data, with high correlation coefficient (r) (Supplementary Table S3). Additionally, in plotting experimental data versus the simulated data (Supplementary Figure S3), we found the relationship to be highly linear with coefficient of variation values also near to 1 (Supplementary Table S3). Quantile-quantile (QQ) plots also indicate that the distributions of simulated and experimental data are comparable, as seen by linear relationships of plotted quantile values individually comparing PVA/PEO and PLGA formulations under 12 or 16 cm dynamic run conditions (Figures 3G,H).

While we conclude these simple simulations can be predictive of actual material deposition, some discrepancies do exist between the theoretical and observed data. These differences

may be due in part to the manual method of controlling electrospinning time to achieve the target basis weight, or from the underlying inconsistency of electrospun fiber deposition in this process format (Collins et al., 2012; Tuin et al., 2016). Root mean square error (RSME) measurements between the experimental and simulated results show that the error is relatively uniform between the tested formulations and dynamic path lengths, except for 16 cm dynamic run PLGA results which have comparatively lower error (Supplementary Table S3). Despite some error, formulation-specific simulations are a valuable tool to determine the required electrospinning parameters needed to achieve the desired area of material at the target basis weight. The methods are especially informative in ensuring sufficient production of drug dosages or devices, while minimizing material waste.

While fibers deposit with gaussian distribution across the MD axis, centered at the wire electrode, the same pattern is not observed across the CD axis. Fibers are generated across the length of the wire (Figure 1B), and therefore the deposition is relatively linear across this length when measured at fixed MD positions (Figure 4). Further, the linear deposition has a near-zero slope. For all linear line fits of mass deposition versus CD position at fixed MD positions, slopes do not significantly deviate from zero with the exception at MD = -4 cm for the PVA/PEO 16 cm dynamic run and for MD = -6 cm for the PLGA static run. Inconsistencies in this linear trend are especially observed for MD cross-sections furthest from the wire, as seen by low basis weight



values for samples collected for MD = 6 or 8 cm at CD = 0 for PVA/PEO 16 cm dynamic run (**Figure 4B**). This is likely due to sampling outside of the uniform area, where mass deposition dramatically decreases (**Figure 3E**). Plots of fiber surface density across the CD-axis further illustrate the differences in spread between the two formulations under static conditions, as seen by the differences in the spread of γ -intercept values (**Figure 4A,C**). Improved consistency under dynamic electrospinning conditions can also be observed as measured by the reduction in γ -intercept range in comparison to statically electrospun materials (**Figures 4A–D**).

Drug Uniformity Across the Sampling Area

Pharmaceutical solid dosage-formulation and agent delivery is one promising application for electrospun biomaterials. Scalable methods of electrospinning would be required for the generation of multiple dosages across a single fiber mat. Furthermore, materials with high basis weight could deliver larger dosages within a smaller material area. We therefore sought to assess the uniformity and encapsulation efficiency of physicochemically diverse pharmaceutical agents within these high basis weight materials. Here, we use three different pharmaceutical agents as model drugs: maraviroc (MVC), raltegravir (RAL), and etravirine

(ETR). These drugs are all antiretroviral agents, but have differences in water-solubility ranging from 0.011 mg/ml (National Center for Biotechnology Information, 2022b), 53.9 mg/ml (National Center for Biotechnology Information, 2022b), and 0.00397 mg/ml (John and Liang, 2014) for MVC, RAL, and ETR, respectively. These drugs also have a range of reported partition coefficients ($\log P$) of 4.3 for MVC (National Center for Biotechnology Information, 2022a), 0.4 for RAL (National Center for Biotechnology Information, 2022b), and >5 for ETR (John and Liang, 2014). Therefore, we expect these agents to represent an interesting challenge for formulation consistency. We prioritized using the optimized PVA/PEO formulation, which are common excipients in many drug delivery systems and where drug dissolution is nearly instantaneous following contact with water. Each drug was loaded into the polymer solution at 5% (w/w), representing a total 15% (w/w) theoretical drug amount within the fibers. Since the target basis weight is 100 gsm, full encapsulation of drug is theoretically equivalent to 5 gsm for each ARV drug. Measurements of percent drug loading approximates drug basis weight but is not necessarily equivalent. We hypothesized that dynamic, free-surface electrospinning could yield multi-drug loaded materials that had uniform basis weight

TABLE 1 | Mass and drug loading averages across a fiber sheet and between fiber sheet replicates.

	Fiber sheet 1	Fiber sheet 2	Fiber sheet 3	Overall
Fiber Mass (gsm)	90.57 ± 3.83	103.0 ± 4.53	97.76 ± 6.81	97.11 ± 7.21
Range (gsm)	85.7–98.3	96.9–111.5	89.6–110.1	85.7–111.5
Range in % error from target	–14.3 to +1.7	–3.1 to +11.5	–10.4 to +10.1	–14.3 to +11.5
% CV	4.231	4.393	6.967	7.429
MVC loading (gsm)	3.88 ± 0.24	3.95 ± 0.58	4.11 ± 0.58	3.98 ± 0.39
MVC range (gsm)	3.55–4.26	2.89–4.55	3.72–4.65	2.89–4.65
Range in % error from target	–28.9 to –14.8	–42.2 to –8.9	–25.6 to –7.0	–42.2 to –7.0
% CV	6.312	14.74	6.458	9.883
RAL loading (gsm)	2.74 ± 0.19	4.22 ± 0.27	3.59 ± 0.29	3.52 ± 0.66
RAL range (gsm)	2.46–3.07	3.83–4.63	3.14–4.00	2.46–4.63
Range in % error from target	–50.8 to –38.6	–23.4 to –7.5	–37.2 to –19.9	–50.8 to –7.5
% CV	7.012	6.294	8.050	18.83
ETR loading (gsm)	4.66 ± 0.25	4.75 ± 0.36	4.68 ± 0.32	4.70 ± 0.30
ETR range (gsm)	4.27–5.01	4.23–5.25	4.28–5.16	4.23–5.25
Range in % error from target	–14.7 to +0.1	–15.3 to +4.9	–14.4 to +3.3	–15.3 to +4.9
% CV	5.381	7.620	6.750	6.461

Target values are equal to 100 gsm for mass and 5 gsm for each drug. Mass and drug measurements reported as average ± standard deviation. Range values reported as min – max. % CV, coefficient of variation. All values determined for just the $-2 < MD < 2$ uniform area ($n = 9$ per mat).

across a defined target area, determined through simulation, and therefore uniform drug basis weight from a single batch process.

Using simulated data, we selected a DPL of 20 cm to create a minimum, proof-of-concept 4 cm MD by 20 cm CD area of fiber uniformity (Figure 5A). The measured mass distribution across multiple replicate fiber sheets correlates to simulated 20 cm dynamic run results (Run 1: Pearson $r = 0.976$; Run 2: $r = 0.981$; Run 3: $r = 0.971$) (Figure 5A). This electrospinning method also proved to be capable of efficiently formulating the three agents into a solid dosage-form, with an average loading efficiency across all measured samples of 82% for MVC, 71% for RAL, and 97% for ETR (Figure 5B). Although highly efficient, specific drug loading is significantly different for the three agents. These differences indicate that hydrophobic drugs formulate more efficiently in this particular formulation. In the predicted uniform area, there is also no significant variation in fiber mass or specific drug loading dependent on location [ex. Center (MD = 0, CD = 0 cm) versus corner (MD = 2, CD = 10 cm)], as determined by comparing averaged replicate values of coordinate defined replicate samples (all $p > 0.16$). This can also be visually observed as even fiber deposition across this center region of the fiber mat (Supplementary Figure S4). Therefore, dynamic free-surface electrospinning can produce uniform drug-loaded materials at the target 100 gsm basis weight.

Representative maps of fiber and drug basis weight distribution are shown for a region encompassing the defined target area and surrounding region within 10% of the simulated target 100 gsm basis weight (Figures 5C–F, all distribution maps are shown in Supplementary Figure S5). Some differences in fiber basis weight and drug loading can be observed for each measurement, however these maps show an overall homogeneity in fiber mass and in each drug across each fiber sheet (Figures 5C–F). While some regions of low drug basis weight may be due to overall reduced mass (Supplementary Figures S5A–D), mass is not the only

driver of drug variation. In some locations, lower drug loading appears to be independent of overall mass deposition (Supplementary Figures S5E–F). Further, some maps indicate lower drug loading across all samples from sheet (Supplementary Figure S5D). However, all measured differences are minimal as determined by a coefficient of variation (CV) of less than 10% for all measurements in the representative fiber mat, and less than 15% for drug measurements in all other replicates (Table 1). These data show the capabilities of the electrospinning process to generate multiple, uniform and high basis weight solid dosage-forms from a single process.

As a proof-of-concept approach to create fiber formulations for sustained drug release, we electrospun MVC, RAL, and ETR at 5% (w/w) each in PLGA. In agreement with simulated and experimental data of PVA/PEO fibers, we used a 20 cm dynamic run to generate a fiber mat with a minimum 4 cm MD by 20 cm CD area of uniform fiber surface density (Supplementary Figure S6A). Unlike the PVA/PEO formulations, polyester formulations were observed to undergo throughput decay, potentially due to the evaporation of solvent in the solution reservoir, known as solution aging. Polyester fibers were also observed to accumulate on the electrospinning carriage during the run, which impeded the ability to reach 100 gsm. As such, we chose 50 gsm as the target basis weight and posit that two mats of controlled surface density could be layered to achieve a higher 100 gsm target. We found that the surface drug distribution of MVC, RAL, and ETR mirrored closely that of the fiber distribution in the MD direction (Supplementary Figure S6B). PLGA fiber uniformity was slightly offset from the 0 cm MD position, likely due to substrate alignment. All three drugs were encapsulated with high efficiency in this uniform region, with an average loading efficiency of 95%, 85%, and 99% for MVC, RAL, and ETR, respectively

(**Supplementary Figure S6C**). This preliminary data on PLGA demonstrates a strong premise for further optimization of high basis weight, uniform, and sustained release solid dosage forms using this fabrication method.

DISCUSSION

To address known shortcomings of electrospinning in application to biomaterial manufacturing, we aim to demonstrate capability for productive fabrication of high basis weight production and uniform materials. Throughput and uniformity are known challenges for electrospinning, potentially due to heterogeneous collection of surface charge, which generates repulsive forces at regions of the material surface (Collins et al., 2012). Low throughput also increases the time and associated cost for material fabrication, thereby limiting the practical clinical translatability of the electrospinning method (Stoddard et al., 2016).

To first assess the impact of free-surface electrospinning parameters on the production of high basis weight materials, we prioritized A) polymer concentration, B) drug loading, C) carriage speed, D) electrode distance, E) electric field, and F) orifice size (**Figure 1**). Polymer concentration significantly impacts fiber production as adequate polymer entanglement is required to form electrospun fibers and avoid electrospinning. However, high viscosity due to high polymer density can also prevent the ability for fibers to form, yet some viscosity is needed to retain polymer solution onto the wire electrode in our electrospinning configuration (Yu et al., 2011). Here, we found that a lower, 0.174 g/ml polymer concentration yielded greater fiber throughput. Drug loading is calculated from the total solid material mass, so increasing drug loading decreases the quantity of polymer available to entangle and form fibers. While drug concentration did not significantly affect either fiber throughput or distribution alone, the interaction between high drug loading and low polymer concentration contributed to greater fiber throughput (**Figure 2C**). This suggests that drug loading of the model agent TVF at ~28% (w/w) did not disrupt polymer entanglement.

In the wire electrospinning-electrode configuration of the Nanospider, the size of the orifice controls the quantity of polymer solution which can coat the wire and the carriage replenishes this polymer coating. Therefore, both orifice and carriage speed affect the volume of solution available to electrospin. Increasing both parameters increased fiber throughput, as well as the interaction of these factors, while carriage speed alone increased the distribution of fibers. In a similar free-surface electrospinning configuration, the rate of rotation into a polymer bath to replenish the liquid polymer coating also showed significant impacts on productivity (Forward and Rutledge, 2012). This study additionally showed that greater applied potential also contributes to greater fiber productivity (Forward and Rutledge, 2012). We also observe greater throughput with a larger electric field, and confirm that the interaction between polymer concentration and electric field are likely significant, with t-values above the t-value limit

(**Supplementary Figure S1**). Increased electric field decreases fiber distribution, which can be rationalized through greater focused attraction of the fibers towards the collection electrode. The distance of the collection electrode, and the interaction between low electric field and increased electrode distance, increases fiber distribution. This can be explained by considering fiber generation from a single jet as an inverted bell curve, with the Taylor Cone at the curve minima. When the substrate is further from the origin of the jet, the width of the distribution increases.

Using the ideal settings of the factors which significantly impacted the assessed outputs, we achieved a maximum fiber throughput rate of 12.9 g/h. Previous research with free-surface electrospinning has focused on fiber throughput as a measure of scalability. The free-surface electrospinning device used in this study, the Nanospider, has been described to achieve a production rate up to 278 g/h (Huang et al., 2019). Free-surface electrospinning has also been described to be capable of up to 1 kg/h production rates (Forward and Rutledge, 2012). However, we are using water as a solvent, which has lower productivity due to a slower evaporation rate compared to organic solvents (Vass et al., 2020). Despite this, aqueous solvents have benefits such as lower cost, compatibility with sensitive agents like biologics, and reduced toxicity from potential residual solvent (Vass et al., 2020). In a similar study using an aqueous solution of PVA and TFV, Krogstad and Woodrow (2014) report a throughput rate of up to 7.6 g/h with wire free-surface electrospinning, while traditional needle electrospinning could only achieve a throughput rate of up to 0.14 g/h. In another free-surface electrospinning study of an aqueous PVA solution, Bhattacharyya, et al. (2015) measured a maximum productivity of approximately 0.5 mg/min per cm of the electrode when characterizing the effect of rotation rate of the electrode on productivity. Our productivity is 8.6 mg/min per cm across a 25 cm wire electrode using our ideal settings. In another study, a yield of 0.0153 g/cm²/h was achieved using polyacrylonitrile dissolved in the organic solvent N,N-dimethylformamide, and electrospun from an open reservoir electrode (Ahmed, et al., 2020). Comparably for our approximately 16 by 16 cm collected fiber area under static conditions, our maximum yield here is 0.05 g/cm²/h. Therefore, our achieved throughput with an aqueous solvent shows acceptable scalable potential. While these optimized settings proved to be productive for these degradable polymers, electrospinning solutions composed of very different formulations, such as protein solutions, may need further assessment.

While production rate is important to characterize for scalability, our focus in this study was to assess the capability of electrospinning to achieve a defined region of high basis weight fiber deposition. The production of high basis weight materials is a challenge for electrospinning due to throughput decay. This reduction of productivity over time can be caused by solution aging, (Forward and Rutledge, 2012; Bhattacharyya et al., 2015; Vass et al., 2020), or by the buildup of residual charges on the collected material surface which can repel fibers (Collins et al., 2012). In a study by Forward and Rutledge (2012), solution aging

limited electrospinning times to only 10 min. We achieved a target basis weight of 100 gsm and show that dynamic electrospinning can create materials with uniform regions of fibers which achieve this high surface density. In our experiments, the run was terminated once the target basis weight was achieved, so this achieved surface density does not represent a maximum limit of this electrospinning method. In the literature, free-surface electrospinning has been reported to achieve a basis weight range of only 0.002–10 gsm (Stoddard et al., 2016; Tuin et al., 2016; Huang et al., 2019). Electrospun materials are commonly characterized as having low basis weight (Yu et al., 2009; Matulevicius et al., 2014; Kadam et al., 2019), and reported values commonly only measure as high as approximately 25 gsm (Wang et al., 2014; Yu et al., 2014; Matulevicius et al., 2016; Opálková Šišková et al., 2020). This is with the exception of a study by Zhang et al. (2017), who report the use of 60 gsm electrospun, acrylonitrile-butadiene materials. Therefore, we present a strategy which yields the highest reported basis weight from electrospinning to our best knowledge. Our achieved basis weight is within the range of other non-woven fabrication methods like meltblowing, spunbond, and carding, which are capable of larger basis weights approximately 5–500, 10–800, or 10–2,000 gsm, respectively. However, electrospinning is also capable of nanosized features, which are approximately 10–100 times smaller than fiber diameters achieved with these alternative methods (Tuin et al., 2016).

Other studies concerning the control over electrospun fiber deposition have mostly focused on alterations to the electric field with collector design (Wu et al., 2007; Feltz et al., 2017; Wang et al., 2017; Creighton et al., 2020). Rather than modifying existing commercial electrospinning equipment to control fiber collection, we present a strategy to regulate the electrospinning process and yield predictable materials. We show that we could control the region of uniform fiber deposition by a simulation-determined DPL, which was dependent on the specific σ_{MD} parameter of the polymer formulation. Simulations used here proved to be a useful tool for determining the minimal run needed to collect the necessary area of uniform material. Methods which can minimize the total run length also minimize the waste of material, drug, and time needed to create the fiber mat. Therefore, the capability to simulate fiber deposition further supports the potential for scalable electrospinning.

We interestingly observed that ETR, which has the lowest water solubility (0.00397 mg/ml (John and Liang, 2014)), also had the highest drug loading (encapsulation efficiency ~97%), and lowest dose variation between all samples (CV ~6.5%) when electrospun in this aqueous solution (**Figure 5B**; **Table 1**) and in an organic solution (**Supplementary Figure S5C**). Hydrophilic drugs have shown poor compatibility with polymers, which has caused known complications for electrospun formulations (Chou et al., 2015; Carson et al., 2016). We therefore consider the >70% encapsulation of hydrophilic RAL to be reasonable. Further, depending on the application, significant differences in loading between drugs may not be a concern or could be accounted for depending on the required relative dosages or specific formulation.

According to United States Pharmacopeia (USP) standards, drug tablets or suppositories are acceptably uniform by content uniformity tests if 10 samples measure within a range of $\pm 15\%$ of the label claim and have a $CV \leq 6\%$, or if all but one in 30 samples falls outside the $\pm 15\%$ range, but all samples are within $\pm 25\%$, and have a $CV \leq 7.8\%$ (Kupiec et al., 2008). In **Table 1** we compare error in drug loading to the full drug loaded into the material as a rigorous measurement of method efficiency, however the label claim refers to the quantity of drug intended for dosing (Kupiec et al., 2008). Although sampling quantities here do not meet the requirements for this assessment, comparisons to these standards can help determine if uniform dosing is possible with electrospun materials, and drug properties which may be the most conducive to uniformity. Across all collected samples, MVC and RAL are not congruent with USP standards, especially when considering dosing error with theoretical loading as the label claim. However, if drug loss is acceptable, and the label claim for MVC is defined as 4.1 gsm (0.32 mg per 1 cm diameter punch), the first and last runs could be considered acceptably uniform for MVC loading. RAL loading shows homogeneity per mat, but inconsistencies per run. Acceptable uniformity would require the label claim to be approximately 2.75 gsm (0.22 mg) RAL for the first run, but 4.25 gsm (0.33 mg) RAL in the second run. The most hydrophobic drug ETR does not exhibit these nonuniformity issues. Even when considering the label claim to be the theoretical loading (5 gsm), ETR dosing in samples across each individual sheet and cumulatively have error within $\pm 15\%$ for all but one sample (at 15.3% error), and a $CV \leq 7.62\%$ (**Table 1**). Therefore, these electrospun materials do show the capability of uniform drug loading comparable to rigorous USP standards.

Although the error of drug encapsulation could be acceptable for some applications, a major shortcoming of this current method is inconsistency across multiple runs potentially due to the manual control over total fiber deposition. Electrospinning throughput rates could be effected by specific volume of polymer within the carriage and environmental factors like humidity (Collins et al., 2012). Further study into such factors could mitigate this error. Variability of hydrophilic drug loading could also be optimized in future studies. Alternative formulations should be assessed if a hydrophilic drug is the target agent for formulation. However, if multiple candidate drugs exist, the selection of a hydrophobic drug may intrinsically improve loading and uniformity in similar electrospun materials. Alternatively, the mapping and interpolation methods presented here could be used to mitigate these issues, as material area could be determined per dose by integrating these drug measurements.

Overall, this study provides in depth characterization of electrospinning parameter effects on throughput and distribution. Moreover, we show that dynamic electrospinning methods could be used to control fiber deposition, and to have a defined region with a uniform target basis weight of 100 gsm. This achieved basis weight is also more than 1.6 times greater than the highest reported surface density for electrospinning to our knowledge (Wang et al., 2014; Yu et al. 2014; Matulevicius et al., 2016; Zhang et al., 2017; Opálková Šišková et al., 2020). While such high-basis weight materials may be ideal for drug

delivery, materials with such density may lack the required porosity for cell permeation into the depth of the material for applications like cell seeding (Annabi et al., 2010; Yu et al., 2011; Collins et al., 2012). Therefore, future alterations to this method, such as porogen loading, could make these electrospun materials further amendable to tissue scaffold relevant biomaterial fabrication. Our methods could also be employed to electrospin materials with other additives, such as graphene particles, as relevant to applications like sensors (Ginestra, et al., 2020). We believe this work presents proof-of-concept capabilities of the electrospinning process to manufacture medical materials. Future work could build upon these methods to further improve particular drug loading and consistency, as relevant to a specific application.

DATA AVAILABILITY STATEMENT

The datasets presented in this study can be found in online repositories. The names of the repository/repositories and accession number(s) can be found below: <http://doi.org/10.17632/swfjyf8g5f.1>.

AUTHOR CONTRIBUTIONS

JH conducted experiments, contributed to project planning, performed data analysis, wrote, and edited the manuscript. M-AD and RS conducted experiments, contributed to project planning, and experimental design. S-TC conducted experiments. IS contributed to project planning and experimental design. KW

REFERENCES

- Ahmed, A., Yin, J., Xu, L., and Khan, F. (2020). High-throughput Free Surface Electrospinning Using Solution Reservoirs with Different Radii and its Preparation Mechanism Study. *J. Mater. Res. Technol.* 9 (4), 9059–9072. doi:10.1016/j.jmrt.2020.06.025
- Annabi, N., Nichol, J. W., Zhong, X., Ji, C., Koshy, S., Khademhosseini, A., et al. (2010). Controlling the Porosity and Microarchitecture of Hydrogels for Tissue Engineering. *Tissue Eng. Part B Rev.* 16 (4), 371–383. doi:10.1089/ten.teb.2009.0639
- Basel Bazbouz, M., Liang, H., and Tronci, G. (2018). A UV-Cured Nanofibrous Membrane of Vinylbenzylated Gelatin-Poly(ϵ -Caprolactone) Dimethacrylate Co-network by Scalable Free Surface Electrospinning. *Mater. Sci. Eng. C* 91, 541–555. doi:10.1016/j.msec.2018.05.076
- Bhattacharyya, I., Molaro, M. C., Braatz, R. D., and Rutledge, G. C. (2016). Free Surface Electrospinning of Aqueous Polymer Solutions from a Wire Electrode. *Chem. Eng. J.* 289, 203–211. doi:10.1016/j.cej.2015.12.067
- Blakney, A. K., Ball, C., Krogstad, E. A., and Woodrow, K. A. (2013). Electrospun Fibers for Vaginal Anti-HIV Drug Delivery. *Antivir. Res.* 100, S9–S16. Elsevier B.V. doi:10.1016/j.antiviral.2013.09.022
- Blakney, A. K., Jiang, Y., and Woodrow, K. A. (2017). Application of Electrospun Fibers for Female Reproductive Health. *Drug Deliv. Transl. Res.* 7 (6), 796–804. doi:10.1007/s13346-017-0386-3
- Blakney, A. K., Simonovsky, F. I., Suydam, I. T., Ratner, B. D., and Woodrow, K. A. (2016). Rapidly Biodegrading PLGA-Polyurethane Fibers for Sustained Release of Physicochemically Diverse Drugs. *ACS Biomater. Sci. Eng.* 2 (9), 1595–1607. doi:10.1021/acsbomaterials.6b00346

provided project planning, guidance with experimental design, and wrote and edited the manuscript. All authors reviewed and provided manuscript feedback.

FUNDING

Research is supported by NIH (National Institutes of Health)/NIAID (National Institute of Allergy and Infectious Disease) 5R01AI145483-04 to KW; the HHMI (Howard Hughes Medical Institute) Gilliam Fellowship for Advanced Study to JH and KW, ARCS (Achievement Rewards for College Scientists) foundation to JH.

ACKNOWLEDGMENTS

We would like to acknowledge the University of Washington Statistical Consulting Service for input on statistical methods. We would also like to thank R. Edmark for all his help with the Nanospider and the electrospinning protocols used here, P. Nguyen for her supporting work with dynamic electrospinning, and C. Everson for his initial guidance with Python.

SUPPLEMENTARY MATERIAL

The Supplementary Material for this article can be found online at: <https://www.frontiersin.org/articles/10.3389/fbiom.2022.928537/full#supplementary-material>

- Botelho Moreira, J. B., Lim, L.-T., Zavareze, E. d. R., Dias, A. R. G., Costa, J. A. V., and Morais, M. G. d. (2019). Antioxidant Ultrafine Fibers Developed with Microalga Compounds Using a Free Surface Electrospinning. *Food Hydrocoll.* 93, 131–136. doi:10.1016/j.foodhyd.2019.02.015
- Carson, D., Jiang, Y., and Woodrow, K. A. (2016). Tunable Release of Multiclass Anti-HIV Drugs that Are Water-Soluble and Loaded at High Drug Content in Polyester Blended Electrospun Fibers. *Pharm. Res.* 33 (1), 125–136. doi:10.1007/s11095-015-1769-0
- Chen, S., Li, R., Li, X., and Xie, J. (2018). Electrospinning: An Enabling Nanotechnology Platform for Drug Delivery and Regenerative Medicine. *Adv. Drug Deliv. Rev.* 132, 188–213. Elsevier B.V. doi:10.1016/j.addr.2018.05.001
- Chou, S.-F., Carson, D., and Woodrow, K. A. (2015). Current Strategies for Sustaining Drug Release from Electrospun Nanofibers. *J. Control. Release* 220, 584–591. Elsevier B.V. doi:10.1016/j.jconrel.2015.09.008
- Collins, G., Federici, J., Imura, Y., and Catalani, L. H. (2012). Charge Generation, Charge Transport, and Residual Charge in the Electrospinning of Polymers: A Review of Issues and Complications. *J. Appl. Phys.* 111 (044701), 044701–044718. doi:10.1063/1.3682464
- Creighton, R. L., Phan, J., and Woodrow, K. A. (2020). *In Situ* 3D-patterning of Electrospun Fibers Using Two-Layer Composite Materials. *Sci. Rep.* 10 (1), 1–14. Springer US. doi:10.1038/s41598-020-64846-z
- Deitzel, J. M., Kleinmeyer, J., Harris, D., and Beck Tan, N. C. (2001). The Effect of Processing Variables on the Morphology of Electrospun Nanofibers and Textiles. *Polymer* 42, 261–272. doi:10.1016/s0032-3861(00)00250-0
- dos Santos, D. M., Correa, D. S., Medeiros, E. S., Oliveira, J. E., and Mattoso, L. H. C. (2020). Advances in Functional Polymer Nanofibers: From Spinning Fabrication Techniques to Recent Biomedical Applications. *ACS Appl. Mat. Interfaces* 12, 45673–45701. doi:10.1021/acsmi.0c12410

- Feltz, K. P., Growney Kalaf, E. A., Chen, C., Martin, R. S., and Sell, S. A. (2017). A Review of Electrospinning Manipulation Techniques to Direct Fiber Deposition and Maximize Pore Size. *Electrospinning* 2 (1), 46–61. doi:10.1515/esp-2017-0002
- Feng, X., Li, J., Zhang, X., Liu, T., Ding, J., and Chen, X. (2019). Electrospun Polymer Micro/nanofibers as Pharmaceutical Repositories for Healthcare. *J. Control. Release* 302, 19–41. Elsevier. doi:10.1016/j.jconrel.2019.03.020
- Forward, K. M., and Rutledge, G. C. (2012). Free Surface Electrospinning from a Wire Electrode. *Chem. Eng. J.* 183, 492–503. Elsevier B.V. doi:10.1016/j.cej.2011.12.045
- Ginestra, P., Riva, L., Fiorentino, A., Zappa, D., Comini, E., and Ceretti, E. (2020). Electrospinning of Poly(vinyl Alcohol)-Graphene Oxide Aligned Fibers. *Procedia CIRP* 89, 110–115. doi:10.1016/j.procir.2020.05.126
- Huang, Y., Song, J., Yang, C., Long, Y., and Wu, H. (2019). Scalable Manufacturing and Applications of Nanofibers. *Mater. Today* 28 (September), 98–113. doi:10.1016/j.mattod.2019.04.018
- Jiang, Y., Cao, S., Bright, D. K., Bever, A. M., Blakney, A. K., Suydam, I. T., et al. (2015). Nanoparticle-Based ARV Drug Combinations for Synergistic Inhibition of Cell-free and Cell-Cell HIV Transmission. *Mol. Pharm.* 12, 4363–4374. doi:10.1021/acs.molpharmaceut.5b00544
- Kadam, V., Kyratzis, I. L., Truong, Y. B., Schutz, J., Wang, L., and Padhye, R. (2019). Electrospun Bilayer Nanomembrane with Hierarchical Placement of Bead-On-String and Fibers for Low Resistance Respiratory Air Filtration. *Sep. Purif. Technol.* 224 (May), 247–254. Elsevier. doi:10.1016/j.seppur.2019.05.033
- Krogstad, E. A., and Woodrow, K. A. (2014). Manufacturing Scale-Up of Electrospun Poly(vinyl Alcohol) Fibers Containing Tenofovir for Vaginal Drug Delivery. *Int. J. Pharm.* 475 (1), 282–291. Elsevier B.V. doi:10.1016/j.ijpharm.2014.08.039
- Kupiec, T. C., Vu, N., and Branscum, D. (2008). Quality-control Analytical Methods: Homogeneity of Dosage Forms. *Int. J. Pharm. Compd.* 12 (4), 340–343.
- LeCorre-Bordes, D. S., Jaksons, P., and Hofman, K. (2017). Mind the Gap: Ensuring Laboratory-Scale Testing of an Electrospinning Product Meets Commercial-Scale Needs. *J. Appl. Polym. Sci.* 134, 1–8. doi:10.1002/app.44836
- Liang, D., and Liang, D. (2014). Oral Liquid Formulation of Etravirine for Enhanced Bioavailability. *J. Bioequiv Availab.* 06 (2), 46–52. doi:10.4172/jbb.1000179
- Matulevicius, J., Kliucininkas, L., Martuzevicius, D., Krugly, E., Tichonovas, M., and Baltrusaitis, J. (2014). Design and Characterization of Electrospun Polyamide Nanofiber Media for Air Filtration Applications. *J. Nanomater.* 2014, 1–13. doi:10.1155/2014/859656
- Matulevicius, J., Kliucininkas, L., Prasauskas, T., Buivydiene, D., and Martuzevicius, D. (2016). The Comparative Study of Aerosol Filtration by Electrospun Polyamide, Polyvinyl Acetate, Polyacrylonitrile and Cellulose Acetate Nanofiber Media. *J. Aerosol Sci.* 92, 27–37. Elsevier. doi:10.1016/j.jaerosci.2015.10.006
- National Center for Biotechnology Information (2022a). PubChem Compound Summary for CID 3002977, Maraviroc, PubChem. Available at: <https://pubchem.ncbi.nlm.nih.gov/compound/Maraviroc> (Accessed: October 12, 2021).
- National Center for Biotechnology Information (2022b). PubChem Compound Summary for CID 54671008, Raltegravir, PubChem. Available at: <https://pubchem.ncbi.nlm.nih.gov/compound/Raltegravir> (Accessed: October 12, 2021).
- Opálková Šišková, A., Frajová, J., and Nosko, M. (2020). Recycling of Poly(ethylene Terephthalate) by Electrospinning to Enhanced the Filtration Efficiency. *Mater. Lett.* 278, 128426. doi:10.1016/j.matlet.2020.128426
- Persano, L., Camposeo, A., Tekmen, C., and Pisignano, D. (2013). Industrial Upscaling of Electrospinning and Applications of Polymer Nanofibers: A Review. *Macromol. Mat. Eng.* 298 (5), 504–520. doi:10.1002/mame.201200290
- Sill, T. J., and von Recum, H. A. (2008). Electrospinning: Applications in Drug Delivery and Tissue Engineering. *Biomaterials* 29 (13), 1989–2006. doi:10.1016/j.biomaterials.2008.01.011
- Skiema, S. S. (2008). *The Algorithm Design Manual*. 2nd edn. New York: Springer. doi:10.1007/978-1-84800-070-4
- Stoddard, R., and Chen, X. (2016). Electrospinning of Ultra-thin Nanofibers Achieved through Comprehensive Statistical Study. *Mat. Res. Express* 3 (5), 055022. doi:10.1088/2053-1591/3/5/055022
- Stoddard, R. J., Steger, A. L., Blakney, A. K., and Woodrow, K. A. (2016). In Pursuit of Functional Electrospun Materials for Clinical Applications in Humans. *Ther. Deliv.* 7 (6), 387–409. doi:10.4155/tde.15.9210.4155/tde-2016-0017
- Tuin, S. A., Pourdeyhimi, B., and Lobo, E. G. (2016). Creating Tissues from Textiles: Scalable Nonwoven Manufacturing Techniques for Fabrication of Tissue Engineering Scaffolds. *Biomed. Mat.* 11, 015017015017. IOP Publishing. doi:10.1088/1748-6041/11/1/015017
- Vass, P., Szabó, E., Domokos, A., Hirsch, E., Galata, D., Farkas, B., et al. (2020). Scale-up of Electrospinning Technology: Applications in the Pharmaceutical Industry. *WIREs Nanomed Nanobiotechnol* 12, 1–24. doi:10.1002/wnan.1611
- Wang, B., Zhou, W., Chang, M.-W., Ahmad, Z., and Li, J.-S. (2017). Impact of Substrate Geometry on Electrospun Fiber Deposition and Alignment. *J. Appl. Polym. Sci.* 134 (19), 1–11. doi:10.1002/app.44823
- Wang, K., Hou, W.-D., Wang, X., Han, C., Vuletic, I., Su, N., et al. (2016). Overcoming Foreign-Body Reaction through Nanotopography: Biocompatibility and Immunoisolation Properties of a Nanofibrous Membrane. *Biomaterials* 102, 249–258. doi:10.1016/j.biomaterials.2016.06.028
- Wang, Y., Li, W., Xia, Y., Jiao, X., and Chen, D. (2014). Electrospun Flexible Self-Standing γ -alumina Fibrous Membranes and Their Potential as High-Efficiency Fine Particulate Filtration Media. *J. Mat. Chem. A* 2, 15124–15131. doi:10.1039/c4ta01770f
- Wu, Y., Carnell, L. A., and Clark, R. L. (2007). Control of Electrospun Mat Width through the Use of Parallel Auxiliary Electrodes. *Polymer* 48 (19), 5653–5661. doi:10.1016/j.polymer.2007.07.023
- Xue, J., Wu, T., Dai, Y., and Xia, Y. (2019). Electrospinning and Electrospun Nanofibers: Methods, Materials, and Applications. *Chem. Rev.* 119 (8), 5298–5415. doi:10.1021/acs.chemrev.8b00593
- Yu, D.-G., Zhu, L.-M., White, K., and Branford-White, C. (2009). Electrospun Nanofiber-Based Drug Delivery Systems. *Health* 01 (02), 67–75. doi:10.4236/health.2009.12012
- Yu, D. G., Branford-White, C., White, K., Chatterton, N. P., Zhu, L. M., Huang, L. Y., et al. (2011). A Modified Coaxial Electrospinning for Preparing Fibers from a High Concentration Polymer Solution. *Express Polym. Lett.* 5 (8), 732–741. doi:10.3144/expresspolymlett.2011.71
- Yu, S., Wang, X., and Wu, D. (2014). Microencapsulation of N-Octadecane Phase Change Material with Calcium Carbonate Shell for Enhancement of Thermal Conductivity and Serving Durability: Synthesis, Microstructure, and Performance Evaluation. *Appl. Energy* 114, 632–643. Elsevier Ltd. doi:10.1016/j.apenergy.2013.10.029
- Zhang, X., Yang, X., and Chase, G. G. (2017). Filtration Performance of Electrospun Acrylonitrile-Butadiene Elastic Fiber Mats in Solid Aerosol Filtration. *Sep. Purif. Technol.* 186, 96–105. Elsevier B.V. doi:10.1016/j.seppur.2017.06.002

Conflict of Interest: The authors declare that the research was conducted in the absence of any commercial or financial relationships that could be construed as a potential conflict of interest.

Publisher's Note: All claims expressed in this article are solely those of the authors and do not necessarily represent those of their affiliated organizations, or those of the publisher, the editors and the reviewers. Any product that may be evaluated in this article, or claim that may be made by its manufacturer, is not guaranteed or endorsed by the publisher.

Copyright © 2022 Hernandez, Doan, Stoddard, VanBenschoten, Chien, Suydam and Woodrow. This is an open-access article distributed under the terms of the Creative Commons Attribution License (CC BY). The use, distribution or reproduction in other forums is permitted, provided the original author(s) and the copyright owner(s) are credited and that the original publication in this journal is cited, in accordance with accepted academic practice. No use, distribution or reproduction is permitted which does not comply with these terms.